Scripta Materialia 162 (2019) 306–310

Contents lists available at ScienceDirect

Scripta Materialia

journal homepage: www.elsevier.com/locate/scriptamat

Enhanced fracture toughness of boron carbide from microalloying and nanotwinning

Yidi Shen [a], Guodong Li [b], Qi An [a,c,*]

[a] Department of Chemical and Materials Engineering, University of Nevada-Reno, Reno, NV 89557, USA
[b] State Key Laboratory of Advanced Technology for Materials Synthesis and Processing, Wuhan University of Technology, Wuhan 430070, China
[c] Nevada Institute for Sustainability, University of Nevada-Reno, Reno, NV 89557, USA

ARTICLE INFO

Article history:
Received 5 October 2018
Received in revised form 15 November 2018
Accepted 17 November 2018
Available online xxxx

Keywords:
DFT
Superhard
Boron carbide
Toughness
Microalloying

ABSTRACT

Fracture toughness is one of the most important mechanical properties of structural materials. Particularly, enhancing the fracture toughness of super-hard materials is essential for their applications. Here, we applied density functional theory to examine how the microalloying and nanotwinning affect the fracture toughness of superhard boron carbide (B_4C). We find that replacing C-B-C chains with two-atom chains especially weakly coupled O atoms can significantly improve the fracture toughness of B_4C. In addition, inserting nanotwins can significantly enhance the fracture toughness of B_4C and boron phases. Our results provide useful information to design boron based superhard materials with enhanced fracture toughness.

Fracture toughness (K_c), describing as the materials capability of resisting cracks propagation, is one of the most important mechanical properties [1,2]. In particular, it is essential to measure and predict the fracture toughness of brittle materials where cracks rather than dislocations and twins are most involved in the mechanical failure and hardness measurement [2]. For decades, many experimental techniques, such as double-torsion [3], fractography [4] and indentation [5–7], have been developed to determine this physical quantity. The choice for measuring fracture toughness depends on resources, availability of time, and level of precision required [7]. Among these techniques, the Vickers indentation fracture (VIF) test, imposing the load from hardness test machine, has been a popular one for brittle materials because of its expediency [5,6]. At a VIF test, the sample generates cracks and the length of cracks, along with elastic modulus, applied load and indent half-diagonal, which are used to determine the fracture toughness of the sample [7].

Besides the above experimental methods, many theoretical studies have predicted the fracture toughness of materials based on various fracture modes [2,8–11]. It is well known that the applied forces on materials could enable a crack to propagate in three ways [11,12]: (1) Mode I, known as opening mode, occurs when the applied tensile stress is normal to the plane of crack; (2) Mode II, known as sliding mode, dominates when the applied shear stress is normal to the leading edge of crack but in the plane of crack; (3) Mode III, known as tearing mode, happens when the applied shear stress is parallel to the leading edge of crack but out of the crack plane. For the materials with Mode I crack, the strength is governed by the Griffth theory in which the theoretical fracture toughness is determined by the relation: $K_{Ic} = 2\sqrt{\gamma_s G/(1-\nu)}$ where ν is Poisson's ratio, G is shear modulus and γ_s is surface energy [13]. However, a fracture toughness K_c measured from experiments is normally considerably different from the theoretical K_{Ic} because defects such as dislocations under shear stress always affect the K_{Ic}. In addition, the dislocations emission is generally a major factor in determining the intrinsic ductile or brittle behaviors of materials [14]. Thus, in order to estimate the resistance of a material to dislocation involved fracture, Rice et al. [9] applied unstable stacking fault energy (γ_{us}) to derive the fracture toughness for Mode II and Mode III: $K_{IIc} = 2\sqrt{\gamma_{us} G/(1-\nu)}$ and $K_{IIIc} = \sqrt{2\gamma_{us} G}$. Although these methods have been established for a decade, their applications to superhard materials are very limited and the accuracy is not well validated.

To significantly accelerate the discovery and optimization of novel superhard materials with enhanced fracture toughness, it is urgent to employ quantum-mechanics (QM) based rational design (in silico optimization) so that the most promising candidates can be identified before experiments. This computational design requires accurate prediction of fracture toughness from QM simulations. To validate the fracture toughness modes, we use boron carbide (B_4C) as a prototype material because of such excellent properties as super strong, low density, high melting point and high abrasion resistance [15–17]. Moreover,

* Corresponding author.
E-mail address: qia@unr.edu (Q. An).

https://doi.org/10.1016/j.scriptamat.2018.11.035
1359-6462/

B_4C has suffered from the brittle failure under impact, characterized by its low fracture toughness, which restrict its extended engineering applications [18–20]. Thus, it is essential to predict the fracture toughness of B_4C and provide rational design to improve it.

The brittle failure of B_4C has been investigated by many theoretical efforts [18,20–27]. In particular, recent studies indicate that the failure of B_4C arises from icosahedra ($B_{11}C$) cracking [18], which leads to the formation of high density amorphous shear bands [21]. Recent theoretical studies suggested that the mechanical behaviors of B_4C can be tuned by nanotwinning or modifying the chain and icosahedral structures (microalloying) [21–27]. However, it is not well established how the fracture toughness was affected by these modifications.

Here, in order to examine how microalloying and nanotwinning affect the fracture toughness of B_4C, we first predicted the theoretical fracture toughness of B_4C and its microalloyed structures of $B_{13}C_2$, $B_{14}C$, B_6O, $B_{12}P_2$, o-$B_{10}Si_2Si_2$. Then, the nanotwinned structures including nanotwinned B_4C (τ-B_4C), B_6O (τ-B_6O) were investigated and compared with their crystalline structures. Finally, we examined the pure boron phases including α-B_{12}, γ-B_{28}, β-B_{106} and τ-B_{106} to illustrate how the various boron structures affect the fracture toughness. Based on our results, the design principles of enhanced toughness of B_4C are established.

It is well established that shear has a weaker resistance against external deformation compared to tension or compression for the selected super-hard materials because their shear modulus is much lower than bulk modulus [24,25,28–32,34]. Thus, we focus on the fracture toughness of Mode II and Mode III in this study. According to previous work by Rice et al. [9], the fracture toughness of Mode II and Mode III fracture could be derived as [9,10]:

$$K_{IIc}^2 = \frac{2\gamma_{us}G}{1-\nu.}$$

$$K_{IIIc}^2 = 2\gamma_{us}G,$$

where ν is Poisson's ratio and can be calculated from bulk modulus (B) and shear modulus (G) through equation: $\nu = \frac{3B-2G}{2(3B+2G)}$. The unstable stacking energy (γ_{us}) can be calculated by integrating the engineering shear-stress-displacement curves which could be derived from the true shear-stress-shear-strain relationships. The detailed estimation method could be found in previous literature [25]. The details of DFT simulations are provided in the supporting information (SI).

To compute the fracture toughness, we first derive the engineering shear-stress-displacement curves from the true shear-stress-shear-strain relationships from the previous shear deformation on selected materials (Fig. S1(a) and Fig. S2 of SI). B_4C and its related compounds τ-B_4C, $B_{13}C_2$, $B_{14}C$, $B_{12}P_2$, τ-B_6O, and o-$B_{10}Si_2Si_2$ have the same plausible slip system of (001)[100] [18,22,23,25,26,28–30](Fig. 1a) while the most plausible slip system for B_6O is changed to (011)[$2\bar{1}\bar{1}$] [24]. For the boron phases of α-B_{12}, β-B_{106}, γ-B_{28} and τ-B_{106}, the most plausible slip system is (001)[$\bar{1}00$] [31–33]. The converted shear-stress-displacement curves for all selected materials are summarized in Fig. 1 (b–d). Then we used the predicted bulk modulus (B) and shear modulus (G) of all selected structures from previous literature, as listed in Table 1 [24,25,28–32,34]. The computed fracture toughness is summarized in Fig. 2 and Table 1.

The low fracture toughness of B_4C arises from its unique crystal structure in which the ground state configuration is $(B_{11}C)^{-1}$-(C-B^+-C) where $B_{11}C$ is the icosahedral cluster and the C-B^+-C represents a 3-atom chain, as shown in Fig. 1(a) [16,18,35,36]. Our predicted fracture toughness of B_4C are K_{IIc} = 1.62 MPa $m^{1/2}$ and K_{IIIc} = 1.47 MPa $m^{1/2}$, which agree well with experimental measurements although the loading conditions are different in experiments and defects exist in experimental samples [33–35]. It is worth to note that the measured fracture toughness in experiments depends on the samples synthesized from different approaches. The measured fracture toughness of fully dense B_4C is 4.7 MPa $m^{1/2}$ based on radial-median cracks [37]. This sample prepared by pressure assisted sintering has a high density and avoids undesirable grain growth, leading to better properties than usual samples. In another experiment, the static mechanical behaviors of spark plasma sintering (SPS) B_4C samples were measured as a function of porosity [38]. The obtained fracture toughness (K_c) is between 3.9 and 4.9 MPa $m^{1/2}$ which were higher than the values reported for samples produced by pressureless sintering and Plasma Pressure Compaction technique (2.8–3.6 MPa $m^{1/2}$) [39,40]. In addition, these experimental values were measured from Vickers indentation experiments in which some uncertainties exist in measuring crack lengths and plastic behaviors beyond critical strain [41]. These uncertainties account for the discrepancy between our theoretical prediction and experimental measurements.

To understand how microalloying affects the fracture toughness of B_4C, we examined the fracture toughness of various B_4C based compounds: B_6O, $B_{12}P_2$, $B_{13}C_2$, $B_{14}C$ and o-$B_{10}Si_2Si_2$. These compounds can be considered as the modification of B_4C. Replacing C atoms in $B_{11}C$ icosahedra leads to the configuration $B_{13}C_2$ and replacing C-B-C chain with C-B-B chain in $B_{13}C_2$ leads to the formation of two $B_{14}C$ configurations: linear chain structure and kink chain structure. The kink chain structure is considered here since it is more stable than linear chain structure. Furthermore, replacing C-B-C chains with oxygen chains (OO) and phosphorus chains (P—P) in $B_{13}C_2$ lead to B_6O and $B_{12}P_2$, respectively. It is worth noticing that two chain oxygen atoms in B_6O are not bonded to each other while P atoms in P—P are bonded to each other [25,30]. Si doping is considered to be a practical approach to improve the ductility of B_4C [23,42]. Here we consider the o-($B_{10}Si_2$)Si_2 compounds in which all C atoms in B_4C are replaced by Si atoms and an additional Si is replacing B in icosahedra to satisfying Wade's rule [29]. Among all these compounds, the fracture toughness of B_6O (K_{IIc} = 2.13 MPa $m^{1/2}$ and K_{IIIc} = 1.96 MPa $m^{1/2}$) and $B_{12}P_2$ (K_{IIc} = 1.77 MPa $m^{1/2}$ and K_{IIIc} = 1.64 MPa $m^{1/2}$) are larger than those of other compounds. Particularly, B_6O shows the highest fracture toughness among all selected compounds. This is because B_6O and $B_{12}P_2$ display larger displacements (Δd = 3.49 Å for B_6O and Δd = 2.78 Å for $B_{12}P_2$) before fracturing compared to other compounds. The large fracture displacements suggest that B_6O and $B_{12}P_2$ are more ductile than other compounds, which is in agreement with our previous studies showing that replacing 3-atoms chain with 2-atoms chain can improve the ductility [25]. In addition to the large displacement, B_6O also has the largest shear modulus (G = 210.9 GPa) among all selected compounds, which also accounts for its highest fracture toughness. It is worth noticing that no icosahedron is broken in $B_{12}P_2$ and B_6O during large shear deformation, making them attractive superhard compounds [25]. For other modified structures, such as $B_{13}C_2$, $B_{14}C$, and o-$B_{10}Si_2Si_2$, their fracture toughness are lower than that of B_4C due to the lower shear modulus or critical shear stress. Their fracture modes are the disintegration of icosahedra, which is similar to B_4C [21,26,28,29]. Particularly, o-($B_{10}Si_2$)Si_2 displays much lower fracture toughness (K_{IIc} = 1.05 MPa $m^{1/2}$ and K_{IIIc} = 0.96 MPa $m^{1/2}$) than those of B_4C (K_{IIc} = 1.62 MPa $m^{1/2}$ and K_{IIIc} = 1.47 MPa $m^{1/2}$), $B_{14}C$ (K_{IIc} = 1.37 MPa $m^{1/2}$ and K_{IIIc} = 1.26 MPa $m^{1/2}$) and $B_{13}C_2$ (K_{IIc} = 1.34 MPa $m^{1/2}$ and K_{IIIc} = 1.20 MPa $m^{1/2}$), as shown in Fig. 2(a). This arises from the very low critical shear stress of o-($B_{10}Si_2$)Si_2, as shown in Fig. 1(b) and Fig. S1(a). These results suggested that it is essential to possess both the large displacement and critical shear stress to achieve high fracture toughness.

Nanotwins has been widely observed in B_4C and related materials [43,44]. In order to understand how nanotwins affect the fracture toughness of B_4C, we examined the fracture toughness of nanotwinned B_4C (τ-B_4C) and B_6O (τ-B_6O), as shown in Fig. 2(b). Comparing the fracture toughness of τ-B_4C with B_4C, we found that even though τ-B_4C shows similar elastic modulus to B_4C (Table 1), the fracture toughness (K_{IIc} = 1.82 MPa $m^{1/2}$ and K_{IIIc} = 1.65 MPa $m^{1/2}$) of τ-B_4C is higher than those of B_4C (K_{IIc} = 1.62 MPa $m^{1/2}$ and K_{IIIc} = 1.47 MPa $m^{1/2}$).

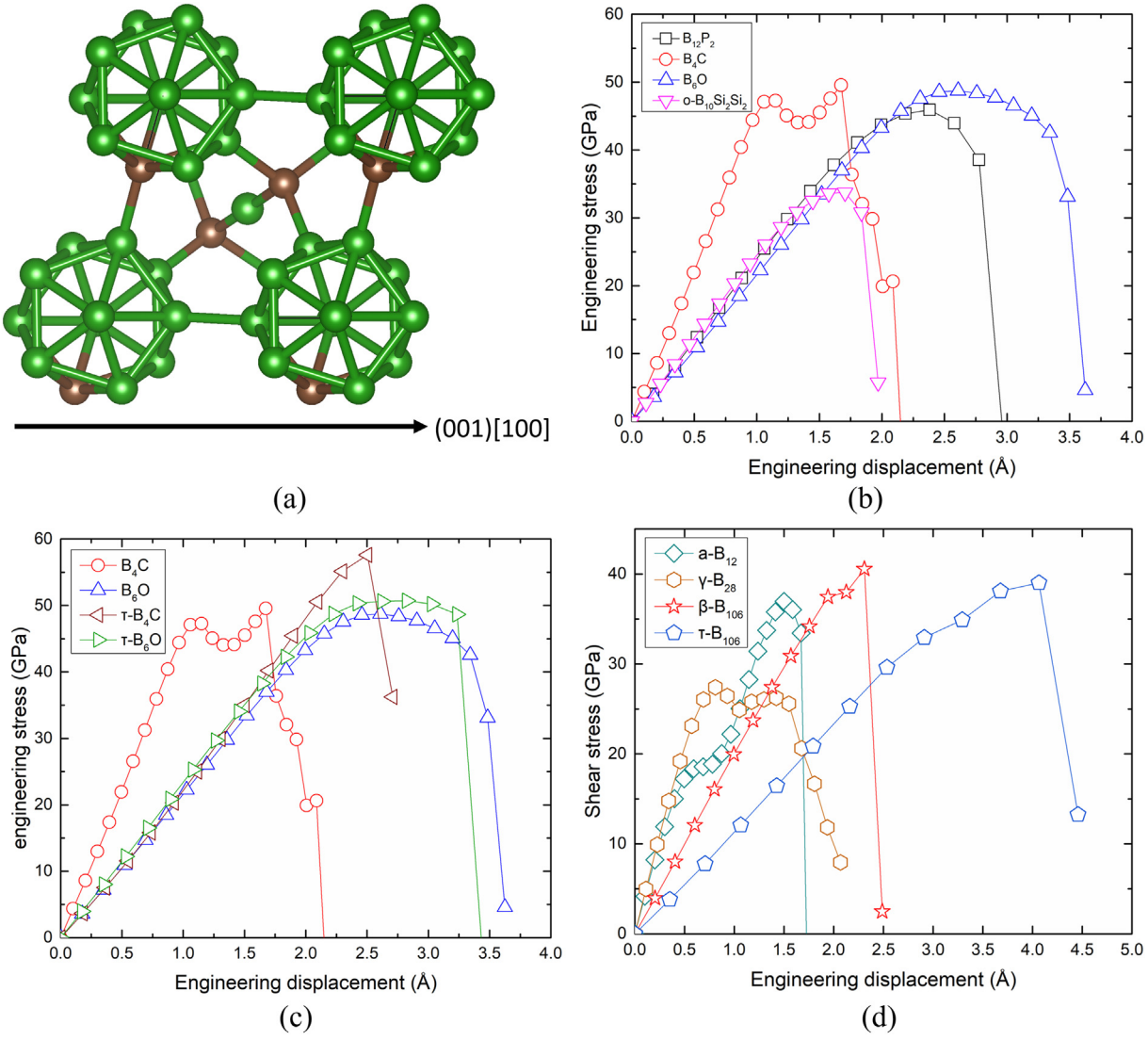

Fig. 1. The structure of B_4C with most plausible slip system of (001)[100] and the ideal engineering shear-stress-displacement relationships for selected superhard materials. (a) The structure of B_4C; (b-d) shear-stress-displacement relationships of (b) the B_4C based compounds including B_4C, B_6O, $B_{12}P_2$ and o-$B_{10}Si_2Si_2$; (c) nanotwinned B_4C (τ-B_4C), B_6O (τ-B_6O); (d) elemental boron phases including α-B_{12}, γ-B_{28}, β-B_{106} and nanotwinned τ-B_{106}.

This is due to the higher critical engineering shear stress of τ-B_4C (57.60 GPa) compared to B_4C (47.26 GPa), as shown in Fig. 1(c). For B_6O, the fracture toughness of nanotwinned B_6O (τ-B_6O) (K_{IIc} = 2.11 MPa $m^{1/2}$ and K_{IIIc} = 1.95 MPa $m^{1/2}$) is very similar to rhombohedral B_6O (K_{IIc} = 2.13 MPa $m^{1/2}$ and K_{IIIc} = 1.96 MPa $m^{1/2}$), as shown in Fig. 2 (b). This suggests that introducing nanotwins in B_6O does not affect the fracture toughness because the τ-B_6O has a slightly shorter displacement (Δd = 3.23 Å) than rhombohedral B_6O (Δd = 3.48 Å) before fracture, as

Table 1
Our estimated bulk modulus (B), shear modulus (G) and fracture toughness of Mode I (K_{Ic}), Mode II (K_{IIc}) and Mode III (K_{IIIc}) for all examined structures. All values of B and G are given in GPa while values of K_{Ic}, K_{IIc} and K_{IIIc} are given in MPa $m^{1/2}$. The V_0 is the equilibrium volume per atom (unit in $Å^3$). A comparison of B and G with previous experimental results is also provided.

Structure	B	G	Experimental B	Experimental G	V_0 ($Å^3$)	K_{Ic}	K_{IIc}	K_{IIIc}
B_4C	238.0	199.0	240[51]	196[52]	7.268	3.029	1.618	1.471
B_6O	232	210.9	222[53]	204[54]	7.386	3.087	2.132	1.964
$B_{12}P_2$	199.1	190.9	192[55]	207[56]	8.782	2.800	1.765	1.640
$B_{13}C_2$	216.3	154.2			7.469	2.553	1.340	1.196
$B_{14}C$	212.3	188.7			7.309	2.788	1.375	1.262
o-($B_{10}Si_2$)Si_2	160.1	136.6			10.620	2.192	1.045	0.956
α-B_{12}	211.7	200.8			7.249	2.868	1.204	1.117
γ-B_{28}	223.0	236.0			6.995	3.173	1.349	1.273
β-B_{106}	204.2	196.7			7.712	2.817	1.476	1.373
τ-B_{106}	202.5	189.1			7.715	2.751	1.962	1.816
τ-B_4C	238.2	197.6			7.270	3.020	1.817	1.650
τ-B_6O	225.9	209.2			7.380	3.033	2.114	1.953

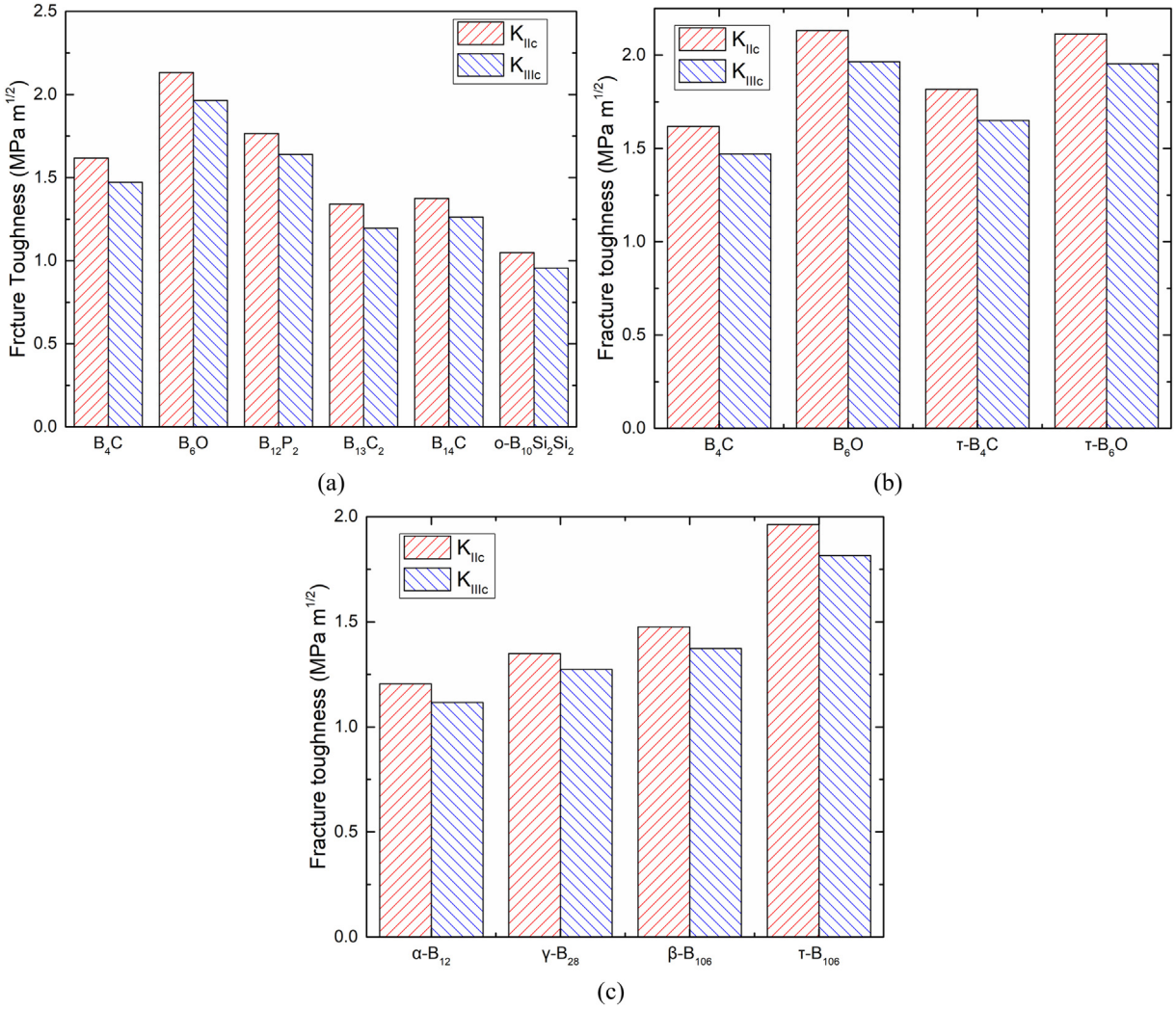

Fig. 2. The estimated fracture toughness of (a) the B_4C based compounds including B_4C, B_6O, $B_{12}P_2$, $B_{13}C_2$, $B_{14}C$ and o-$B_{10}Si_2Si_2$; (b) nanotwinned B_4C (τ-B_4C), B_6O (τ-B_6O); (c) elemental boron phases including α-B_{12}, γ-B_{28}, β-B_{106} and nanotwinned τ-B_{106}.

shown in Fig. 1(c). Thus, it is likely that introducing nanotwins in B_4C improves its fracture toughness, but it does not have much effects in B_6O.

The B_4C crystal structure is the modification of α-B_{12} phase. To understand how the fracture toughness is affected by other possible boron structures, we also examined the fracture toughness of various boron phases, as shown in Fig. 2(c). We consider α-B_{12}, β-B_{106} and γ-B_{28} phases which have been identified as the most stable pure phases [45–47]. Comparing to α-B_{12} (B_{12} icosahedron), the γ-B_{28} has a crystal structure containing two B_{12} icosahedra and two B_2 pairs in the unit cell [32]. For β-B_{106}, the structure is very complex with 106 atoms and partially occupied sites (POS) in the unit cell, in which the main units are B_{12} icosahedra and icosahedral fused B_{28} clusters [48,49]. In addition, our recent study combined high resolution transmission electron microscopy (HRTEM) and QM simulation identified a β-B_{106} transformed twinlike structure, named τ-B_{106} [33]. Here, we examined the fracture toughness of these four boron phases. Comparing the fracture toughness of these structures, the sequence from high to low is τ-B_{106} > β-B_{106} > γ-B_{28} > α-B_{12}, as shown in Fig. 2(c). The τ-B_{106} with twinlike structure exhibits larger fracture toughness than those of other three boron phases because it undergoes larger elastic deformation before fracture, as shown in Fig. 1(d). The engineering shear stress increases to its maximum at the displacement Δd = 4.065 Å, which is much larger than those of other three boron phases. This indicates that nanotwins in elemental boron can improve its fracture toughness. In addition, the β-B_{106} shows a much higher fracture toughness (K_{IIc} = 1.48 MPa $m^{1/2}$ and K_{IIIc} = 1.37 MPa $m^{1/2}$) compared to other two crystalline phases due to its larger critical shear strength (40.56 GPa) and critical displacement (Δd = 2.308 Å) compared to γ-B_{28} (26.06 GPa, Δd = 0.809 Å) and α-B_{12} (36.97 GPa, Δd = 1.671 Å) before fracturing, as shown in Fig. 2(c). Even though γ-B_{28} has the largest shear modulus (236.0 GPa) among these four boron phases, its lowest ideal shear strength lowers the fracture toughness, as shown in Fig. 1(d). However, its fracture toughness is still higher than that of α-B_{12}.

Our results provide useful information of improving the ductility of B_4C. To achieve the enhanced ductility of B_4C under shearing loading, it is essential to (1) replacing the 3-atoms chains with 2-atoms chains; and (2) introducing the nanotwins in B_4C.

It is interesting to predict the theoretical fracture toughness of Mode I fracture (K_{Ic}) for these superhard materials and compare with K_{IIc} and K_{IIIc}. Here we computed the K_{Ic} of B_4C based materials using the recent developed method by Niu et al. [50] as below equation:

$$K_{Ic} = {V_0}^{1/6} \times G \times \left(\frac{B}{G}\right)^{1/2}$$

where V_0 is the equilibrium volume per atom, B is the bulk modulus and G is the shear modulus.

The obtained K_{Ic} for all selected materials are listed in Table 1. For the microalloying effects on B_4C, the K_{Ic} of B_6O (3.09 MPa m1/2) is higher than that of B_4C (3.03 MPa m1/2) because of its larger shear modulus

(G = 210.9 GPa) than that of B_4C (199.0 GPa). The K_{Ic} of o-$B_{10}Si_2Si_2$ displays the lowest K_{Ic} (2.19 MPa m1/2) among all compounds due to the lowest shear modulus (G = 136.6 GPa). These results agree well with our theoretical predictions on the fracture toughness from Mode II and III fracture.

For nanotwinned structures, the K_{Ic} of B_4C and B_6O are similar to those of perfect crystal, indicating that inserting nanotwins into these two materials does not have much effect on K_{Ic}. This is consistent with K_{IIc} and K_{IIIc} for B_4C. While for B6O, the K_{IIc} and K_{IIIc} of τ-B_6O are higher than those of B_6O.

For the pure boron phases, the sequence of K_{Ic} from high to low is γ-B_{28} > α-B_{12} > β-B_{106} > τ-B_{106}, which is accordance with the sequence of shear modulus. While for K_{IIc} and K_{IIIc}, the sequence from high to low is τ-B106 > β-B106 > γ-B28 > α-B12.

The comparison suggests that the fracture toughness of Mode I fracture mainly depends on shear modulus. It is worth to notice that this K_{Ic} prediction only depends on the elastic modulus and equilibrium volume. Application of this approach on superhard materials needs to be validated by comparing experiments and theoretical predictions.

In summary, we predict the fracture toughness of B_4C, its microalloyed structures, the nanotwinned structures τ-B_4C, τ-B_6O, and four pure boron phases using DFT simulations. Under shear loading, among all crystalline structures, B_6O and $B_{12}P_2$ exhibit higher fracture toughness than other compounds due to large displacement before fracture. For nanotwinned structures, τ-B_4C display higher fracture toughness than its crystal structures because of its higher critical engineering shear stress, while the fracture toughness of τ-B_6O is similar to rhombohedral B_6O because τ-B_6O has a shorter range of displacement before fracture. For pure boron phases, τ-B_{106} exhibits the highest fracture toughness because of large elastic deformation. Our results suggest that (1) replacing C-B-C chains with two-atom chains especially weakly coupled O atoms can significantly enhance the fracture toughness of B_4C; (2) nanotwins can be applied to improve the fracture toughness of B_4C and elemental boron.

Acknowledgement

This work is supported by National Science Foundation (CMMI-1727428).

Appendix A. Supplementary data

Supplementary material includes additional information on computational methodology, engineering shear-stress-displacement curves for all crystalline structures and shear-stress-shear-strain curves for all selected materials. Supplementary data associated with this article can be found in the online version, at doi: https://doi.org/10.1016/j.scriptamat.2018.11.035.

References

[1] M. Guazzato, M. Albakry, S.P. Ringer, M.V. Swain, Dent. Mater. 20 (2004) 449–456.
[2] Z. Ding, S. Zhou, Y. Zhao, Phys. Rev. B 70 (2004) 184117.
[3] R.B. Tait, P.R. Fry, G.G. Garrett, Exp. Mech. 27 (1987) 14–22.
[4] R.E. Campos, C.J. Soares, P.S. Quagliatto, P.V. Soares, O.B. de Oliveira, P.C.F. Santos-Filho, S.M. Salazar-Marocho, J. Prosthodont. 20 (2011) 447–455.
[5] S. Jayaraman, G.T. Hahn, W.C. Oliver, C.A. Rubin, P.C. Bastias, Int. J. Solids Struct. 35 (1998) 365–381.
[6] G.D. Quinn, R.C. Bradt, J. Am. Ceram. Soc. 90 (2007) 673–680.
[7] W.C. Wagner, T.M. Chu, J. Prosthet. Dent. 76 (1996) 140–144.
[8] D. Tromans, J.A. Meech, Miner. Eng. 15 (2002) 1027–1041.
[9] J.R. Rice, J. Mech. Phys. Solids 40 (1992) 239–271.
[10] G. Li, U. Aydemir, S.I. Morozov, S.A. Miller, Q. An, W.A. Goddard, P. Zhai, Q. Zhang, G.J. Snyder, Acta Mater. 149 (2018) 341–349.
[11] A. Karma, D.A. Kessler, H. Levine, Phys. Rev. Lett. 87 (2001) 045501.
[12] Q. Rao, Z. Sun, O. Stephansson, C. Li, B. Stillborg, Int. J. Rock Mech. Min. Sci. 40 (2003) 355–375.
[13] E. Rocha-Rangel, Fracture Toughness Determinations by Means of Indentation Fracture, 2011.
[14] A. Kelly, W.R. Tyson, A.H. Cottrell, Philos. Mag. 15 (1967) 567–586.
[15] G. Fanchini, J.W. McCauley, M. Chhowalla, Phys. Rev. Lett. 97 (2006) 035502.
[16] V. Domnich, S. Reynaud, R.A. Haber, M. Chhowalla, J. Am. Ceram. Soc. 94 (2011) 3605–3628.
[17] M. Chen, J.W. McCauley, K.J. Hemker, Science 299 (80) (2003) 1563–1566.
[18] Q. An, W. Goddard, T. Cheng, Phys. Rev. Lett. 113 (2014) 095501.
[19] H. Kim, Y.-H. Koh, H.-E. Kim, J. Am. Ceram. Soc. 83 (2000) 2863–2865.
[20] K.M. Reddy, P. Liu, A. Hirata, T. Fujita, M.W. Chen, Nat. Commun. 4 (2013) 2483.
[21] Q. An, W.A. Goddard, Phys. Rev. Lett. 115 (2015) 105501.
[22] Q. An, W.A. Goddard, K.Y. Xie, G.D. Sim, K.J. Hemker, T. Munhollon, M. Fatih Toksoy, R.A. Haber, Nano Lett. 16 (2016) 7573–7579.
[23] Q. An, W.A. Goddard, J. Phys. Chem. Lett. 5 (2014) 4169–4174.
[24] Q. An, K.M. Reddy, H. Dong, M.W. Chen, A.R. Oganov, W.A. Goddard, Nano Lett. 16 (2016) 4236–4242.
[25] Q. An, W.A. Goddard, Chem. Mater. 27 (2015) 2855–2860.
[26] Q. An, W.A. Goddard, Appl. Phys. Lett. 110 (2017) 111902.
[27] C. Cheng, K.M. Reddy, A. Hirata, T. Fujita, M. Chen, J. Eur. Ceram. Soc. 37 (2017) 4514–4523.
[28] X. Yang, W.A. Goddard, Q. An, J. Phys. Chem. C 122 (2018) 2448–2453.
[29] Q. An, W.A. Goddard III, J. Phys. Chem. C 121 (2017) 11831–11838.
[30] Q. An, W.A. Goddard, J. Phys. Chem. C 121 (2017) 16644–16649.
[31] Q. An, S.I. Morozov, Phys. Rev. B 95 (2017) 064108.
[32] Q. An, W.A. Goddard, H. Xiao, T. Cheng, Chem. Mater. 26 (2014) 4289–4298.
[33] Q. An, K.M. Reddy, K.Y. Xie, K.J. Hemker, W.A. Goddard, Phys. Rev. Lett. 117 (2016) 085501.
[34] Q. An, Phys. Rev. B 95 (2017) 100101.
[35] D. Gosset, M. Colin, J. Nucl. Mater. 183 (1991) 161–173.
[36] N. Vast, J. Sjakste, E. Betranhandy, J. Phys. Conf. Ser. 176 (2009) 012002.
[37] D. He, Y. Zhao, L. Daemen, J. Qian, T.D. Shen, T.W. Zerda, Appl. Phys. Lett. 81 (2002) 643–645.
[38] W. Ji, S.S. Rehman, W. Wang, H. Wang, Y. Wang, J. Zhang, F. Zhang, Z. Fu, Sci. Rep. 5 (2015) 15827.
[39] B.M. Moshtaghioun, D. Gomez-Garcia, A. Dominguez-Rodriguez, R.I. Todd, J. Eur. Ceram. Soc. 36 (2016) 1829–1834.
[40] H. Lee, R.F. Speyer, J. Am. Ceram. Soc. 85 (2002) 1291–1293.
[41] L. Liu, N. Ogasawara, N. Chiba, X. Chen, J. Mater. Res. 24 (2009) 784–800.
[42] A.U. Khan, A.M. Etzold, X. Yang, V. Domnich, K.Y. Xie, C. Hwang, K.D. Behler, M. Chen, Q. An, J.C. Lasalvia, K.J. Hemker, W.A. Goddard, R.A. Haber, Acta Mater. 157 (2018) 106–113.
[43] H. Dong, A.R. Oganov, Q. Wang, S.N. Wang, Z. Wang, J. Zhang, M.M.D. Esfahani, X.F. Zhou, F. Wu, Q. Zhu, Sci. Rep. 6 (2016) 31288.
[44] K.Y. Xie, Q. An, M.F. Toksoy, J.W. McCauley, R.A. Haber, W.A. Goddard, K.J. Hemker, Phys. Rev. Lett. 115 (2015) 175501.
[45] A.R. Oganov, J. Chen, C. Gatti, Y. Ma, Y. Ma, C.W. Glass, Z. Liu, T. Yu, O.O. Kurakevych, V.L. Solozhenko, Nature 457 (2009) 863–867.
[46] R.E. Hughes, C.H.L. Kennard, D.B. Sullenger, H.A. Weakliem, D.E. Sands, J.L. Hoard, J. Am. Chem. Soc. 85 (1963) 361–362.
[47] A.R. Oganov, V.L. Solozhenko, J. Superhard Mater. 31 (2009) 285–291.
[48] S. Hayun, V. Paris, M.P. Dariel, N. Frage, E. Zaretzky, J. Eur. Ceram. Soc. 29 (2009) 3395–3400.
[49] M.A. White, A.B. Cerqueira, C.A. Whitman, M.B. Johnson, T. Ogitsu, Angew. Chem. Int. Ed. 54 (2015) 3626–3629.
[50] H. Niu, S. Niu, A.R. Oganov, Simple and Accurate Model of Fracture Toughness of Solids, arXiv, 1805, 2018 05820.
[51] S.P. Dodd, G.A. Saunders, C. Lane, S.K.T. Oee, J. Mater. Sci. 37 (2002) 2731–2736.
[52] K.J. McClellan, F. Chu, J.M. Roper, I. Shindo, J. Mater. Sci. 36 (2001) 3403–3407.
[53] M.C. Tushishvili, C.V. Tsagareishvili, D.S.J. Tsagareishvili, Hard Mater. 99 (1992) 225–233.
[54] D.M. Teter, MRS Bull. 23 (1998) 22–27.
[55] V.L. Solozhenko, K.A. Cherednichenko, O.O. Kurakevych, J. Superhard Mater. 39 (2017) 71–74.
[56] Y. Gao, M. Zhou, H. Wang, C. Ji, C.E. Whiteley, J.H. Edgar, H. Liu, Y. Ma, J. Phys. Chem. Solids 102 (2017) 21–26.